CrossMark

ORIGINAL ARTICLE

Vorticity dynamics after the shock–turbulence interaction

D. Livescu[1] · J. Ryu[2]

© Springer-Verlag Berlin Heidelberg (outside the USA) 2015

Abstract The interaction of a shock wave with quasi-vortical isotropic turbulence (IT) represents a basic problem for studying some of the phenomena associated with high speed flows, such as hypersonic flight, supersonic combustion and Inertial Confinement Fusion (ICF). In general, in practical applications, the shock width is much smaller than the turbulence scales and the upstream turbulent Mach number is modest. In this case, recent high resolution shock-resolved Direct Numerical Simulations (DNS) (Ryu and Livescu, J Fluid Mech 756:R1, 2014) show that the interaction can be described by the Linear Interaction Approximation (LIA). Using LIA to alleviate the need to resolve the shock, DNS post-shock data can be generated at much higher Reynolds numbers than previously possible. Here, such results with Taylor Reynolds number approximately 180 are used to investigate the changes in the vortical structure as a function of the shock Mach number, M_s, up to $M_s = 10$. It is shown that, as M_s increases, the shock interaction induces a tendency towards a local axisymmetric state perpendicular to the shock front, which has a profound influence on the vortex-stretching mechanism and divergence of the Lamb vector and, ultimately, on the flow evolution away from the shock.

Communicated by A. Podlaskin.

✉ D. Livescu
livescu@lanl.gov

1 CCS-2, Los Alamos National Laboratory, Los Alamos, NM 87545, USA

2 Department of Mechanical Engineering, University of California, Berkeley, CA 94720, USA

1 Introduction

The interaction of shock waves with turbulence is an important aspect in many types of flows, from hypersonic flight, to supersonic combustion, to astrophysics and Inertial Confinement Fusion (ICF). In general, the shock width is much smaller than the turbulence scales, even at low shock Mach numbers, M_s, and it becomes comparable to the molecular mean free path at high M_s values. When there is a large scale separation between the shock and turbulence, viscous effects become negligible during the interaction. If, in addition, the turbulent Mach number, M_t, of the upstream turbulence is small, the nonlinear effects can also be neglected during the interaction. In this case, the interaction can be treated analytically using the linearized Euler equations and Rankine–Hugoniot jump conditions. This is known as the Linear Interaction Approximation (LIA) [1–3]. However, due to the high cost of simulations for the parameter space close to the LIA limit (and practical applications) and difficulties with accurate experimental measurements close to the shock, previous studies have shown only limited agreement with LIA [3–10]. Recently, Ryu and Livescu [11], using high resolution fully resolved Direct Numerical Simulations (DNS) extensively covering the parameter range, have shown that the DNS results converge to the LIA solutions as the ratio δ/η, where δ is the shock width and η is the Kolmogorov microscale of the incoming turbulence, becomes small. The results reconcile a long time open question about the role of the LIA theory and establish LIA as a reliable prediction tool for low M_t turbulence–shock interaction problems. Furthermore, when there is a large separation in scale between

🖄 Springer

the shock and the turbulence, the exact shock profile is no longer important for the interaction, so that LIA can be used to predict arbitrarily high M_s interaction problems, when the Navier–Stokes equations are no longer valid and fully resolved DNS are not feasible.

The shock–turbulence interaction has been traditionally studied in an open-ended (shock-tube) domain, with the turbulence fed through the inlet plane encountering a stationary shock at some distance from the inlet. Usually, turbulence has been generated either directly in the inlet plane or with additional decaying isotropic turbulence (IT) simulations and then used in the spatial domain by invoking the Taylor hypothesis. To avoid this hypothesis, which limits the magnitude of the acoustic component and overall turbulence intensity to small values, Ryu and Livescu [11] have generated the inlet turbulence in separate forced compressible IT simulations with background velocity matching the shock speed and using the linear forcing method [12] (Fig. 1). This forcing method has the advantage of specifying the Kolmogorov micro scale and ratio of dilatational to solenoidal kinetic energies, χ, at the outset. Nevertheless, the shock-tube approach is very expensive (with or without realistic inlet turbulence), even when a shock-capturing scheme is used, and limited to low Taylor Reynolds numbers, Re_λ. However, the range of the achievable Re_λ values can be significantly increased if, instead, one uses the LIA theory to generate the post-shock fields. To be able to generate full 3-D fields, Ryu and Livescu [11] have extended the classical LIA formulas, which traditionally have been used to calculate second order moments only. Using this procedure, they showed profound changes in the structure of post-shock turbulence, with significant potential implications on turbulence modeling.

The analysis of small amplitude fluctuations in a compressible medium performed by Kovasznay [13] showed the existence of three basic modes: the vorticity, acoustic and entropy modes. For uniform mean flow, in the inviscid limit, the modes evolve independently. The vortical and entropy modes are advected by the mean flow, while the acoustic mode travels at the speed of sound. The vortical mode consists in a solenoidal velocity field only, the entropic mode only has density and temperature fluctuations while the acoustic mode has isentropic pressure and density fluctuations and a corresponding irrotational (dilatational) velocity that satisfies the acoustic wave equation. Thus, the velocity field has contributions from the acoustic and vortical modes, the density and temperature fields from acoustic and entropic components and the pressure field is only associated with the acoustic mode. The interaction with the shock generates all three modes, even when the upstream turbulence has only one mode present. In many practical applications, the intensity of the upstream turbulence fluctuations is small enough that the fast interaction with a thin shock is in the linear regime
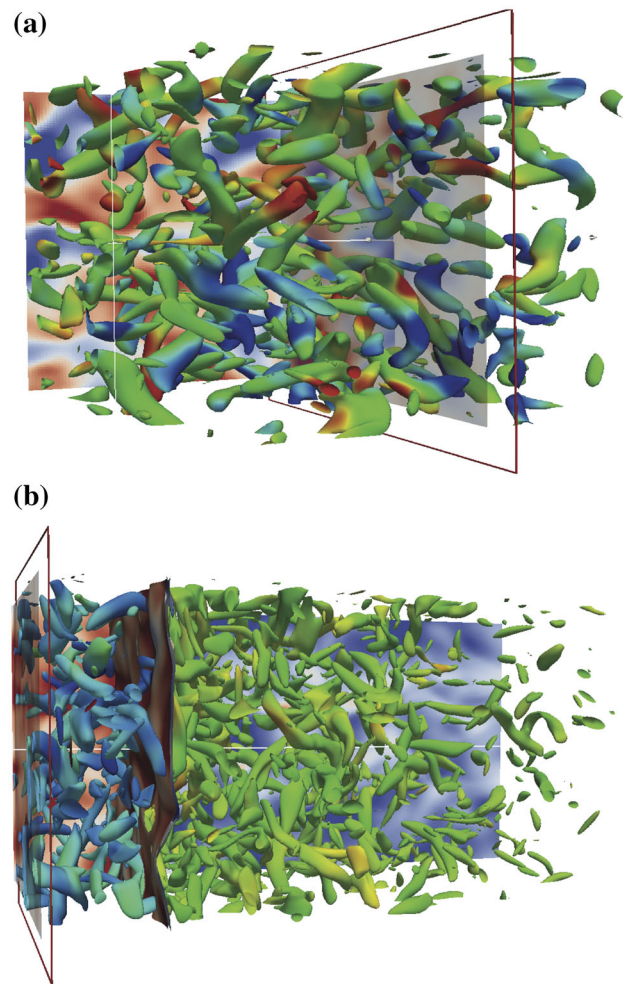

(a)

(b)

Fig. 1 Numerical setup for DNS of shock–turbulence interaction in Ref. [11]: data recorded from forced IT simulations with background velocity matching the shock speed **a** are fed through the inlet of an open-ended domain **b**. The *red rectangle* is the plane where the flow data are recorded **a** and the location of inlet feeding **b**. Eddy structures are visualized by the Q-criterion

[11]; however, the flow evolution away from the shock occurs over much longer time and length scales and nonlinear and viscous effects can no longer be neglected. In this case, the three modes become fully coupled [14,15]. Nevertheless, the evolution following the interaction with the shock, be it pure decay or subsequent interactions, depends on the properties of the post-shock turbulence.

While recent shock–turbulence interaction studies [9,10] using shock-capturing techniques or full DNS [11] have significantly extended the range of Reynolds numbers achieved in such a flow (~70 for shock capturing and ~45 for full DNS), the Re_λ values are still smaller than those considered necessary to reach the transition to fully developed turbulence. For example, IT is considered to be fully developed if $Re_\lambda > 100$ [16], although much larger values may be needed if higher order statistics are investigated. In addition, previous

studies have examined in detail various quantities related to the transport equations for the second order moments, such as Reynolds stresses (e.g. [9,10]). Ryu and Livescu [11] have extended the analysis of the post-shock fields to the local properties of the strain rate tensor, **S**. Yet, there are still many gaps in our knowledge of post-shock turbulence, for example concerning the vorticity field, such as the vortex-stretching mechanism and its relation to the energy cascade and the Lamb vector and its connection with coherent structures.

Simulations of turbulent flows with shocks have to contend with contradictory requirements for the numerical algorithms to simultaneously capture the turbulence and the shocks. Thus, turbulence simulations require the minimization of numerical dissipation for small scale representation, while the shocks require increased local dissipation to regularize the algorithm [17]. Explicit subgrid models also need to account for the presence of the shock. Yet, available high Re_λ data necessary to investigate the turbulence models are scarce.

This study aims at using the novel procedure proposed by Ryu and Livescu [11] to generate high Re_λ post-shock data and study the properties of post-shock turbulence, as reflected in the characteristics and dynamics of the vorticity field. First, the results are shown to be consistent with our extensive DNS database for up to $M_s = 2.2$ and then used to predict the characteristics of the vorticity field after the shock and its downstream evolution at high M_s values. Here, the incoming turbulence is vortical; results with incoming turbulence having significant entropic and acoustic modes will be presented elsewhere.

The paper is organized as follows. Section 2 contains the governing equations, problem setup and the numerical methodology, as well as the extended LIA formulas. Section 3 is the main results section of the paper. Thus, Sect. 3.1 shows the convergence of the DNS enstrophy amplification to the LIA prediction, Sect. 3.2 discusses the vorticity field and the vortex-stretching mechanism, Sect. 3.3 focuses on the Lamb vector and its divergence and Sect. 3.4 provides some data on the correlation between vorticity and the thermodynamic variables. Finally, Sect. 4 provides the conclusions.

2 Problem setup and numerical methods

The equations considered for studying the properties of post-shock turbulence are the compressible Navier–Stokes equations with the perfect gas assumption [12]. The ratio of specific heats is $\gamma = 1.4$, the viscosity varies with the temperature as $\mu = \mu_0 (T/T_0)^{0.75}$, and the Prandtl number is $Pr = 0.7$. All simulations use the compressible version of the CFDNS code [11,12,18]. The setup for the DNS of the shock–turbulence interaction (Fig. 1) is described in detail in Ref. [11].

In order to generate high Re_λ post-shock data, forced compressible IT simulations are performed first. The forcing procedure, proposed in Ref. [12], is the same as that used for the DNS of the shock–turbulence interaction in Ref. [11]. Then the turbulent fields, instead of being fed through the inlet of the shock-tube, are passed through the LIA formulas. Thus, by alleviating the need to resolve the shock in the shock-tube simulations, much higher Reynolds number turbulence data can now be used. For this paper, the forced turbulence simulations are performed on 512^3 domains, with $\eta/\Delta x = 0.8$ (for which the differentiation error is small compared to a spectral simulation with $\eta k_{max} = 1.5$ [12]), $\chi = 0.01$ (quasi-vortical upstream turbulence) and $M_t = 0.05$. For this upstream turbulent Mach number, the downstream ratio between the turbulent, M_{t2}, and mean flow, M_{s2}, Mach numbers is less than 0.1, indicating small nonlinear effects during the interaction [11]. Also, the ratio $\delta/\eta \simeq 7.69 M_t/(Re_\lambda^{0.5}(M_s - 1))$ is around 0.14 for the smallest ($M_s = 1.2$) and 0.003 for the largest ($M_s = 10$) M_s value considered. The forced turbulence simulations yield a Reynolds number $Re_\lambda \simeq 180$, which is much larger than previous shock-tube simulations (with or without shock capturing) and above the transition to fully developed turbulence.

2.1 Linear interaction analysis

Traditional LIA only requires information about the upstream turbulence spectrum shape and provides solutions for the second-moment statistics behind the shock wave. To compute full post-shock flow fields, which are necessary for higher order statistics, one needs full flow fields in front of the shock as well. These fields are taken from separate three-dimensional forced IT calculations described above. First, the velocity components are Fourier transformed in all three physical directions (x, y, z), and each Fourier mode with (k_x, k_y, k_z) wavenumber component is related to the two-dimensional plane wave in the traditional LIA by a spherical coordinate transformation: $k = \sqrt{k_x^2 + k_y^2 + k_z^2}$, $k_x = k \cos \psi$, and $k_z = k_y \tan \phi$. Here, the wavenumber k_x is in the direction perpendicular to the shock wave and the two-dimensional plane wave lies in the plane formed by the x direction and the wave vector $\mathbf{k}$. Then, k, ψ, and ϕ are, respectively, the wavelength of the plane wave, the angle between the wave vector and x direction and the angle between the y axis and the plane of the wave. In this study, we focus on the interaction of a shock wave with vortical turbulence. The Helmholtz decomposition [15] is used to remove the small dilatational part of the upstream velocity, which is less than 1% of the total kinetic energy ($\chi = 0.01$). This small magnitude component does not affect the overall numerical results; however, the vortical LIA formulas rely on zero divergence

of velocity. In order to be able to apply the LIA procedure, the velocity vector is decomposed into a component lying in the plane of the wave, $\mathbf{u}_{\parallel}$, and a component perpendicular to the plane of the wave, $\mathbf{u}_{\perp}$. For non-interacting plane waves, the latter acts as a constant background velocity, parallel to the shock wave, which should pass unchanged through the shock [1]. Thus, for small M_t values, the full 3-D turbulence fields can be decomposed into a collection of non-interacting plane waves, which follow the LIA theory [1,2], each with an additional velocity component which remains unchanged through the shock.

The velocity vector in the plane of the wave is perpendicular to the wave vector and has a complex velocity amplitude $A_v = \hat{u}_x^s / \sin \psi$, where $\hat{u}_x^s$ is the Fourier coefficient of the solenoidal streamwise velocity disturbance. The complex amplitude of $\mathbf{u}_{\perp}$ can be written as $u_{\perp} = -\hat{u}_y^s \sin \phi + \hat{u}_z^s \cos \phi$, where $\hat{u}_y^s$ and $\hat{u}_z^s$ are the Fourier coefficients of the solenoidal transverse velocity fluctuations.

Then, for given M_s values, the post-shock velocity disturbances are

$$u'_x = \int_{k=0}^{\infty} \int_{\psi=0}^{\pi} \int_{\phi=0}^{2\pi} A_v \left\{ \tilde{F} e^{i\tilde{k}x} + \tilde{G} e^{ik_x rx} \right\} \Gamma k^2 dV_s, \quad (1)$$

$$u'_y = \int_{k=0}^{\infty} \int_{\psi=0}^{\pi} \int_{\phi=0}^{2\pi} \left\{ A_v \cos \phi \left[\tilde{H} e^{i\tilde{k}x} + \tilde{I} e^{ik_x rx} \right] \right.$$
$$\left. - u_{\perp} \sin \phi e^{ik_x rx} \right\} \Gamma k^2 dV_s, \quad (2)$$

$$u'_z = \int_{k=0}^{\infty} \int_{\psi=0}^{\pi} \int_{\phi=0}^{2\pi} \left\{ A_v \sin \phi \left[\tilde{H} e^{i\tilde{k}x} + \tilde{I} e^{ik_x rx} \right] \right.$$
$$\left. + u_{\perp} \cos \phi e^{ik_x rx} \right\} \Gamma k^2 dV_s, \quad (3)$$

where $\tilde{k}$ is the post-shock acoustic wavenumber, r is the ratio of the upstream and downstream mean streamwise velocities, $\Gamma = e^{i(k_y y + k_z z)}$, $dV_s = \sin \psi d\phi d\psi dk$, and $\tilde{F}$, $\tilde{G}$, $\tilde{H}$ and $\tilde{I}$ are the LIA coefficients. Note that ψ and ϕ are varied from 0 to π and from 0 to 2π, respectively, to consider the full flow field; whereas ψ is varied from 0 to $\pi/2$ and the ϕ variation is not considered in the traditional LIA due to the symmetry and homogeneity of the second-moment statistics with the angles. Also, the $u_{\perp}$ contribution does not appear in the final formulas for the Reynolds stresses but it needs to be included when considering the full flow fields. The formulas for the density and pressure fluctuations behind the shock can be found in Ref. [3]. $\tilde{k}$ is the root of the quadratic equation which is derived from the pressure wave equation behind the shock wave. The root which corresponds to the physical solution is chosen; the other root implies either exponentially growing or upstream propagating acoustic wave behind the

shock wave. For $\psi < \psi_c$ and $\psi > \pi - \psi_c$, $\tilde{k}$ is real; the $+$ sign is chosen for the former and $-$ sign for the latter. ψ_c is the critical angle at which the term under the square root is zero. The derivatives with respect to ψ have an infinite discontinuity at ψ_c, due to the divergence of the $\tilde{k}$ derivative. The solutions themselves are continuous with a cusp at ψ_c, which leads to a much larger amplification at ψ_c. Physically, as $\tilde{k}$ changes from real to complex at ψ_c, the acoustic solution acquires a decaying component in the streamwise direction and the downstream velocity in a frame of reference moving along the shock with velocity V changes from supersonic to subsonic [1]. The moving velocity V is chosen such that the disturbance velocity in the plane of the wave does not change its direction through the shock.

The definitions of the LIA coefficients are presented below. The complete derivation of these coefficients can be found in Refs. [1–3]. Here, the final formulas are shown as required by the extended procedure.

$$\tilde{F} = \alpha D_1 (l - \tilde{L}), \quad (4)$$
$$\tilde{G} = \tilde{L}(1 - B_1) - \tilde{F} + B_1 l, \quad (5)$$
$$\tilde{H} = \beta D_1 (l - \tilde{L}), \quad (6)$$
$$\tilde{I} = -\frac{mr}{l}(1 - B_1 + \alpha D_1)\tilde{L} + mr\alpha D_1 - mr B_1, \quad (7)$$

where

$$\alpha = \frac{1}{\gamma r^2 M_{s_2}^2} \frac{\tilde{k}/k}{m - \tilde{k}/(kr)}, \quad (8)$$

$$\beta = \frac{1}{\gamma r^2 M_{s_2}^2} \frac{l}{m - \tilde{k}/(kr)}, \quad (9)$$

$$B_1 = \frac{(\gamma - 1)M_s^2 - 2}{(\gamma + 1)M_s^2}, \quad (10)$$

$$D_1 = \frac{4\gamma M_s^2}{2\gamma M_s^2 - (\gamma - 1)}, \quad (11)$$

$$E_1 = \frac{2(M_s^2 - 1)}{(\gamma + 1)M_s^2}, \quad (12)$$

$$\tilde{L} = \frac{-m - \beta D_1 l - mr\alpha D_1 + mr B_1}{E_1 l^2 - \beta ml D_1 - m^2(1 - B_1 + \alpha D_1)} ml, \quad (13)$$

$m = \cos \psi$, $l = \sin \psi$, γ is the ratio of specific heats, M_{s_2} is the mean Mach number behind the shock, which is given by the Rankine–Hugoniot relations, and, finally,

$$\tilde{k} = \frac{-m \pm 1/M_{s_2} \sqrt{m^2 - (1/M_{s_2}^2 - 1)l^2/r^2}}{1/M_{s_2}^2 - 1} kr. \quad (14)$$

It is noted that the formulas above do not require isotropy, so they can be applied to anisotropic turbulence as well.

3 Results and discussion

The properties of post-shock turbulence, as related to several aspects of the vorticity field, are examined below. First, a discussion is provided for the convergence of the DNS results for enstrophy amplification to the traditional LIA prediction. These results use the DNS database generated in Ref. [11]. Then, high Re_λ post-shock turbulence data are analyzed using the new forced compressible IT fields and extended LIA formulas described above.

Below, Shock-LIA and Shock-DNS refer to the post-shock fields computed using the extended LIA theory and DNS, respectively. The Shock-DNS results for the vorticity amplification are calculated at the shock, for comparison with previous studies. Those results are averaged in time and over the transverse directions. However, note that enstrophy remains constant after the shock in Shock-LIA. The Shock-LIA results correspond to the plane of maximum amplification of the streamwise Reynolds stress, which occurs approximately at $k_0 x = \pi$. Here, $k_0 = 1$ is the wavenumber of the peak of the kinetic energy spectrum (the forcing wavenumber for the forced turbulence simulations). At $k_0 x = \pi$, the variations in the mean fields become small in a corresponding shock-tube DNS, so that the contributions from the mean flow to the turbulence quantities discussed here are small. Physically, this location corresponds to the end of the inviscid adjustment of the acoustic component, following the shock–turbulence interaction, after which the LIA statistics become spatially constant. The region of agreement between DNS and LIA can be extended into this constant regime, provided that δ/η and M_t are small enough, since the eddy turnover time and, consequently, the decay distance increase with decreasing M_t at fixed Re_λ [11]. Note that features of the evolution away from the shock, like return to isotropy, cannot be captured by the LIA solutions. However, such effects due to nonlinear interactions can be made arbitrarily small by decreasing M_t. The Taylor Reynolds number for Shock-LIA is $\text{Re}_\lambda = 180$ and for shock-DNS it varies between 10 and 45.

3.1 Enstrophy amplification

As the scale separation between the shock wave width and the turbulence scales becomes large, for small upstream M_t values, the viscous and nonlinear effects become negligible during the interaction process, even at relatively low Re_λ values. In this case, the DNS results should be close to the LIA prediction. Ref. [11] showed that the results can become fully converged for the streamwise variation of the Reynolds stresses and enstrophy in a region close to the shock wave, even at $\text{Re}_\lambda \leq 45$. The extent of this region increases as the scale separation increases. Since for upstream IT the ratio of the shock width to Kolmogorov microscale is given by
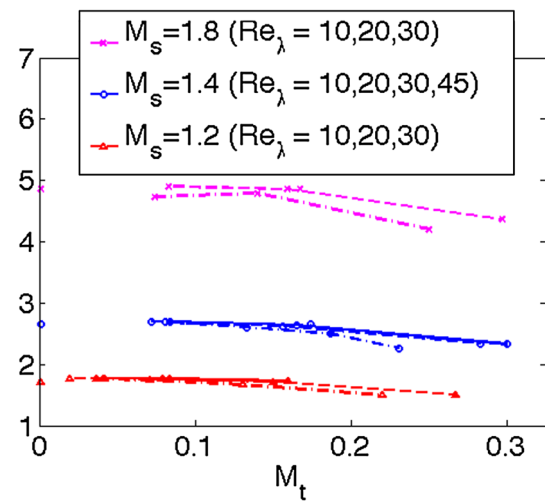

Fig. 2 Convergence of Ω_{tr} amplification to the LIA solution for different values of Re_λ. In this figure only, the results are calculated at the shock, for comparison with previous studies. *Symbols* along the vertical axis represent the LIA solution with the shape and color matched for the symbol-lines of corresponding M_s. Higher Re_λ cases are located above the corresponding lower Re_λ cases. Additional results can be found in Ref. [11]

$\delta/\eta \simeq 7.69 M_t/(\text{Re}_\lambda^{0.5}(M_s - 1))$, the scale separation can be arbitrarily increased at a fixed Re_λ value by decreasing the turbulent Mach number. Figure 2 shows the transverse enstrophy amplification, $\Omega_{\text{tr}} = \langle \omega_y^2 + \omega_z^2 \rangle^d / \langle \omega_y^2 + \omega_z^2 \rangle^u$, where the exponents ^{d} and ^{u} represent the values immediately downstream and upstream of the shock and $\boldsymbol{\omega} = \nabla \times \mathbf{u}$ is the vorticity, for some of the DNS cases discussed in Ref. [11]. The amplifications, as well as the streamwise variation immediately following the shock (not shown here), become fully converged to the LIA solutions for the Re_λ values accessible in DNS. The convergence region includes the location of the streamwise Reynolds stress maximum amplification and extends into the region where the LIA statistics become spatially constant. When the enstrophy amplification converges to the LIA solutions, it no longer changes as the Reynolds number is increased (Fig. 2).

The traditional LIA procedure calculates second order moments of the turbulence fields, which require information about the incoming turbulence spectra only. Thus, higher order correlations characterizing the turbulence fields and their change through the shock cannot be predicted by the usual LIA formulas. In principle, formulas to predict higher order moments could be derived from (1)–(3); however, these formulas would require knowledge about higher order moments upstream of the shock as well and involve increasingly cumbersome convolution products. The procedure used here, with full flow fields ahead of the shock, provides full information downstream of the shock. Figure 3 shows the Probability Density Function (PDF) of the transverse velocity component, normalized by the corresponding enstrophy
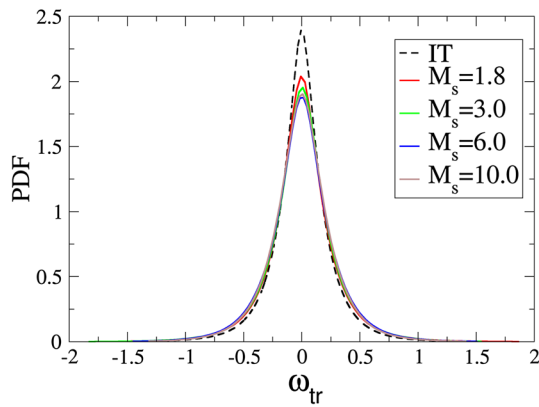
Fig. 3 PDF of transversal vorticity component. All Shock-LIA PDFs are normalized by $\sqrt{\Omega_{tr}}$, so that they have the same variance as the IT PDF
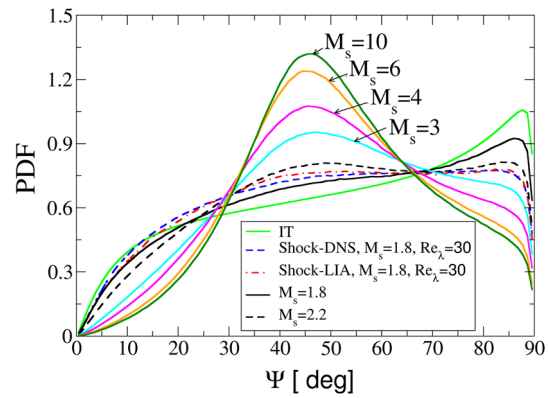

Fig. 4 PDF of the strain-enstrophy angle Ψ (degrees). The $Re_\lambda = 30$ results are obtained from the database of Ref. [11]. The present results have $Re_\lambda = 180$

jump. Any departure from the IT profile after the normalization is reflective of the contributions from the higher order correlations. The largest differences occur around the peak of the PDF and at lower M_s values. After $M_s = 6$, the changes in the PDF are small.

3.2 Vorticity field and the vortex-stretching mechanism

While the DNS results converge to the LIA predictions even at low Reynolds numbers, investigating post-shock turbulence properties requires Reynolds numbers large enough that the upstream turbulence is fully developed. The results presented below are obtained using the Shock-LIA procedure, with $Re_\lambda \approx 180$. Some comparisons are made with the database from Ref. [11] using both Shock-DNS and the corresponding Shock-LIA results from the $M = 1.8$ run with $Re_\lambda \simeq 30$, which had $\delta/\eta \simeq 0.3$.

The LIA relations show that the shock interaction amplifies preferentially the transverse components of the rotation and strain stress tensor [3,11]. This leads to an increase in the correlation between the two quantities as M_s increases [11,19]. Ref. [11] provides some information based on the joint PDF of the strain and rotation tensors magnitudes. In order to investigate this behavior in more detail and also assess the Reynolds number influence, Fig. 4 shows the PDF of the strain-enstrophy angle, Ψ, defined as [20]:

$$\Psi = \tan^{-1} \frac{S_{ij}S_{ij}}{W_{ij}W_{ij}} \tag{15}$$

where the strain and rotation tensors components are given by $S_{ij} = \frac{1}{2}(A_{ij} + A_{ij})$ and $W_{ij} = \frac{1}{2}(A_{ij} - A_{ij})$, respectively, with $A_{ij} = \partial u_i/\partial x_j$. By definition, large values of Ψ ($\gg 45°$) correspond to strain dominance and small values ($\ll 45°$) correspond to rotation dominance. The regions with $\Psi \sim 45°$ are the highly correlated regions. In IT, the PDF of Ψ peaks

at large values, consistent with previous results [20,21]. This behavior can be seen even at relatively low Reynolds numbers. However, after the shock interaction, some differences in low and high Reynolds number behavior start to appear. As the Mach number increases, the PDF becomes more symmetrical, with a stronger peak at $\Psi = 45°$. Nevertheless, the tails of the PDF remain asymmetric, as there are still more regions of strain dominance compared to rotation dominance. The low Reynolds number results with $M_s = 1.8$, while showing good agreement between Shock-DNS and Shock-LIA, tend to underestimate these regions (Fig. 4).

In most fully developed 3-D turbulent flows, there is a preferential alignment between the vorticity vector and the eigenvectors of the strain rate tensor [22–24]. This is due to the local dynamics of vorticity and strain rate tensor, and can be affected by several mechanisms, e.g. the formation of distinct spatial structures [25] or by heat release due to the enhancement of dilatational motions or local decrease in Reynolds number [21,26]. Thus, the vorticity vector tends to align with the intermediate (β-) eigenvector and there is no preference with respect to the most extensive (α-) eigenvector. The eigenvectors correspond to the eigenvalues α, β and γ, denoted with the usual convention that $\alpha > \beta > \gamma$. For quasi-vortical vortical upstream turbulence, $\alpha + \beta + \gamma = A_{ii} \simeq 0$. Figure 5 shows that IT turbulence results are consistent with the previous studies. However, in post-shock turbulence, the alignment with the β-eigenvectors strengthens and there is a tendency towards a local alignment with the vorticity perpendicular to the α- and γ- eigenvectors as M_s increases. Here, the angles ζ_1, ζ_2 and ζ_3 correspond to the α-, β- and γ-eigenvectors, respectively. The enhancement of the alignment with the β-eigenvector was also found in Ref. [19]. This change in alignment is due to a preferential amplification of the transverse vorticity and strain rate tensor components due to the compression in the shock normal direction.
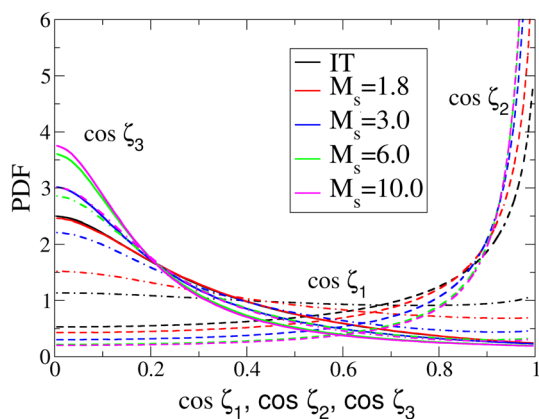
Fig. 5 PDF of cosines of the angles between $\boldsymbol{\omega}$ and the eigenvectors of the strain rate tensor, **S**: $\cos \zeta_1$, *dash dotted lines*, $\cos \zeta_2$, *dashed lines*, $\cos \zeta_3$, *solid lines*

Fig. 6 PDF of cosine of the angle between **a** $\boldsymbol{\omega}$ and **b** β-eigenvector with the streamwise direction

Indeed, Fig. 6 shows that both vorticity and the β-eigenvector are increasingly aligned at a 90° angle with the shock normal (streamwise) direction, as M_s increases. At the same time (not shown) the other two eigenvectors tend to align in the shock normal direction. In fully developed turbulence, there is no preferential orientation of the inertial range structures with the coordinate directions, consistent with the IT results in Fig. 6. However, the interaction with the shock changes the turbulence at all scales and vorticity and strain rate eigenvectors acquire a strong directionality with the coordinate directions. Post-shock turbulence is no longer fully developed 3-D turbulence, there is a tendency, amplified as M_s increases, towards an axisymmetric (2-D) local state.

The state and structure of post-shock turbulence are very important for the evolution away from the shock. The changes in the orientation of vorticity and strain rate eigenvectors will give rise to various transients, until a fully developed state is again reached. Some consequences of these changes can be highlighted by considering the transport equation for the enstrophy:

$$\frac{\partial \langle \Omega \rangle}{\partial t} + \langle \nabla \cdot (\mathbf{v}\Omega) \rangle = \langle \boldsymbol{\omega} \cdot \mathbf{S} \cdot \boldsymbol{\omega} \rangle - \langle \Omega \nabla \cdot \mathbf{v} \rangle$$
$$- \left\langle \boldsymbol{\omega} \cdot \left(\frac{\nabla p \times \nabla \rho}{\rho^2} \right) \right\rangle + \left\langle \boldsymbol{\omega} \cdot \left(\nabla \times \left[\frac{\nabla \cdot \boldsymbol{\tau}}{\rho} \right] \right) \right\rangle, \quad (16)$$

where $\Omega = |\boldsymbol{\omega}|^2/2$ and $\boldsymbol{\tau}$ represents the stress tensor. [4,5,27] analyzed this equation to explain the evolution of the vorticity through the shock. Here, the focus is on the consequences of the changes in the turbulence structure behind the shock for the evolution downstream of the shock. The terms on the right hand side (RHS) of (16) represent vortex-stretching, vorticity-expansion, production due to baroclinic torque and viscous dissipation. During the evolution through the shock, the variations in the mean fields give most of the contribu-
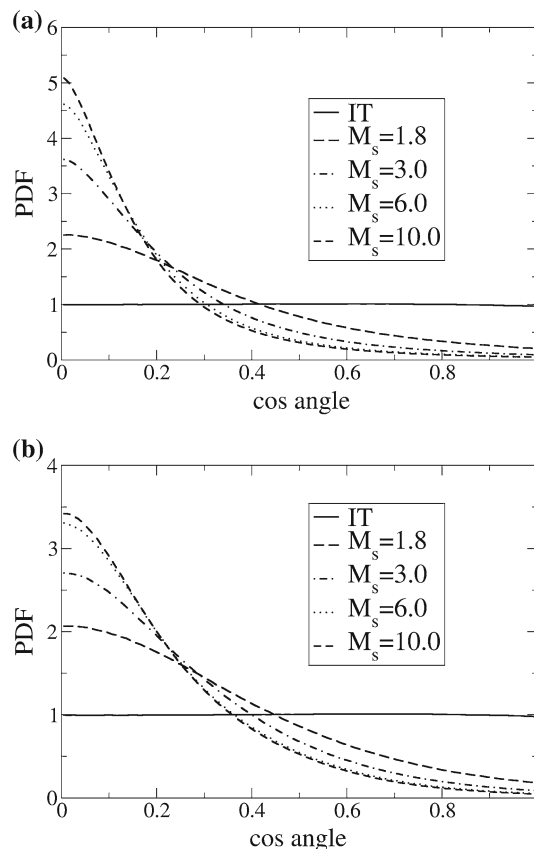
tions to the terms in (16). Thus, vortex-stretching and viscous terms are negligible and the advection, vorticity-expansion and baroclinic terms are dominant [27]. However, after the shock interaction, for the case of upstream vortical turbulence, these terms become small and are not discussed here, although we note that both are amplified as M_s increases, in both absolute magnitude and relative to the upstream fields.

The two important terms in (16) after the shock interaction with quasi-vortical turbulence are vortex-stretching and viscous terms. The vortex-stretching term is a fundamental aspect of 3-D turbulence and is intimately related to the energy cascade to small scales. Due to the change in the orientation of both vorticity and strain rate eigenvectors and tendency towards a local axisymmetric state, an important question is about the effect on the vortex-stretching mechanism. This term can be expressed using the eigenvectors and eigenvalues of **S** as:

$$\langle \boldsymbol{\omega} \cdot \mathbf{S} \cdot \boldsymbol{\omega} \rangle = \left\langle |\boldsymbol{\omega}|^2 \left(\alpha \cos^2 \zeta_\alpha + \beta \cos^2 \zeta_\beta + \gamma \cos^2 \zeta_\gamma \right) \right\rangle$$
$$(17)$$

As both $\cos^2 \zeta_\alpha$ and $\cos^2 \zeta_\gamma$ are larger after the shock (Fig. 5), there is an increasing cancelation between the first and last
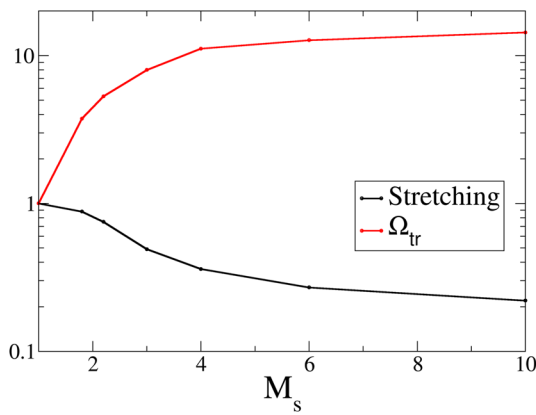
Fig. 7 Amplification of transverse vorticity variance and vortex-stretching term in the enstrophy equation, normalized by Ω_{tr}, turbulence time scale and the corresponding IT value

contributions to vortex-stretching, while the increased alignment with the β-eigenvector does not play a role since the β eigenvalue has small magnitude. Nevertheless, the enstrophy and α and γ eigenvalues increase substantially in magnitude due to the compression in the shock normal direction. This leads to an amplification in the absolute value of the vortex-stretching term after the shock interaction. However, after the normalization by the enstrophy and turbulence time scale, $\tau = K/\epsilon$, where $K = R_{ii}/2$ is the turbulent kinetic energy, $R_{ij} = \langle u_i u_j \rangle$ are the Reynolds stresses and ϵ is the dissipation, Fig. 7 shows that vortex-stretching becomes substantially lower than in IT. As a result, on the time scale of the turbulence, the flow may take a much longer time, compared to a similar non-shocked flow, to return to a 3-D, fully developed state. This tendency is stronger at higher M_s values, indicating a slower rate of return; however, the changes are less significant as M_s increases above 6.

3.3 The Lamb vector

The advection, vortex-stretching and vortex-expansion terms in (16) can be grouped together using the Lamb vector, $\mathbf{l} \equiv \boldsymbol{\omega} \times \mathbf{v}$:

$$\boldsymbol{\omega} \cdot \nabla \times \mathbf{l} = \nabla \cdot (\mathbf{v}\Omega) - \boldsymbol{\omega} \cdot \mathbf{S} \cdot \boldsymbol{\omega} + \Omega \nabla \cdot \mathbf{v} \qquad (18)$$

The Lamb vector also appears in the momentum equation, if the advection term is re-written as:

$$(\mathbf{v}\nabla) \cdot \mathbf{v} = \boldsymbol{\omega} \times \mathbf{v} + \nabla^2 K \qquad (19)$$

and in the transport equation for the divergence of velocity, $\Delta \equiv A_{i,i}$:

$$\frac{\partial \langle \Delta^2 \rangle}{\partial t} = -\langle \Delta \nabla \cdot \mathbf{l} \rangle - \langle \Delta \nabla^2 K \rangle$$
$$+ \left\langle \Delta \left(\frac{\nabla p \cdot \nabla \rho}{\rho^2} \right) \right\rangle + \left\langle \nabla \cdot \left[\frac{\nabla \cdot \tau}{\rho} \right] \right\rangle \qquad (20)$$

In incompressible turbulence, the Lamb vector and its divergence have been intensely studied, e.g. since it is solely responsible for the total force acting on a moving body or due to the connection to the description of coherent structures [28]. Negative values of $\nabla \cdot \mathbf{l}$ are interpreted as spatially localized motions that have accumulated the capacity to introduce a time rate of change in momentum. On the contrary, positive values represent motions with a depleted such capacity. The divergence of the Lamb vector can be written as:

$$\nabla \cdot \mathbf{l} = \mathbf{u} \cdot \nabla \times \boldsymbol{\omega} - \boldsymbol{\omega} \cdot \boldsymbol{\omega}, \qquad (21)$$

so that $\nabla \cdot \mathbf{l}$ can be positive only when the flexion product, $F \equiv \mathbf{u} \cdot \nabla \times \boldsymbol{\omega}$ is positive. Since the Lamb vector acts as a vortex force, the Lamb vector divergence identifies inhomogeneities in the momentum transport surrounding a fluid element, or a flux of energy, that propagates or concentrates local energy curvature. In a region of flow where the flexion product is positive, the enstrophy acts as a storage mechanism and the flexion product behaves like a release mechanism of the momentum flux and kinetic energy. In addition, the interaction between the flexion product and enstrophy gives rise to an energy curvature interpretation and minimization process for interactions occurring in many incompressible flows. In compressible flows, while some interesting phenomena, such as the connection with the Bernoulli equation, are lost, we note the additional connection between $\nabla \cdot \mathbf{l}$ and the production of dilatational motions (see equation 20). In addition, $\nabla \cdot \mathbf{l}$ plays a key role in the production of jet noise whenever its mean is different than zero [29]. Compressible generalizations for the force acting on a body using the Lamb vector have also been attempted (e.g. [30]).

In both IT and post-shock turbulence, the flexion product has both positive and negative values, but the PDF is skewed to the right (Fig. 8). As the Mach number increases, the magnitude of F also increases considerably. Perhaps more interesting is the connection between the flexion product and velocity divergence (Fig. 9). In IT, the two quantities are uncorrelated, as reflected in the joint PDF. However, in post-shock turbulence, the regions with the largest flexion product values occur predominantly in the compression regions ($\Delta < 0$). Following the transport equation for the square of the divergence, it is likely that the strongest compression regions will be further amplified during the initial stages of the evolution away from the shock. The energy released from these regions should continue to enhance the small scale activity, in addition to the decrease of the Kol-
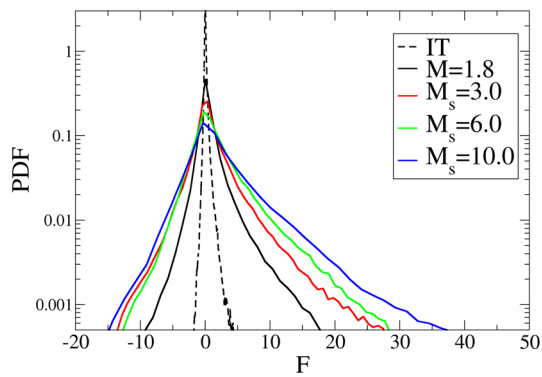
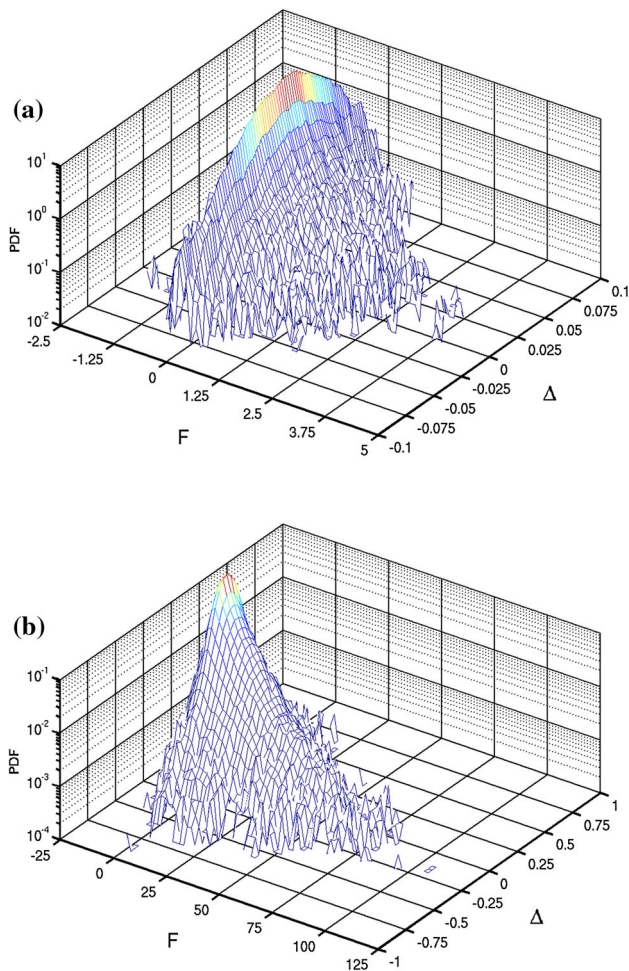**Fig. 8** PDF of the flexion product

Fig. 9 Joint PDF of the flexion product and divergence of velocity **a** IT and **b** post-shock turbulence with $M_s = 10$

mogorov microscale due to the direct interaction with the shock.

3.4 Thermodynamic variables

One characteristic of the interaction with the shock is that, even if only one of the three compressible modes is present
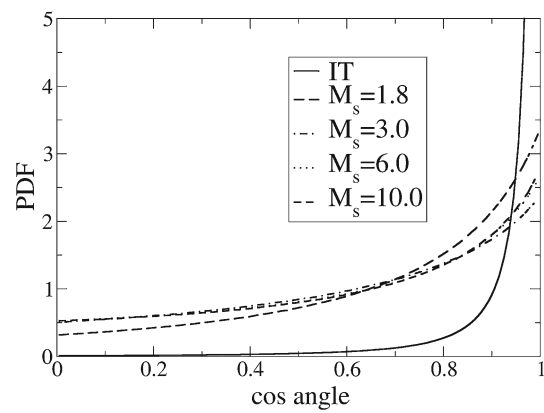

Fig. 10 PDF of cosine of the angle between the pressure and density gradients
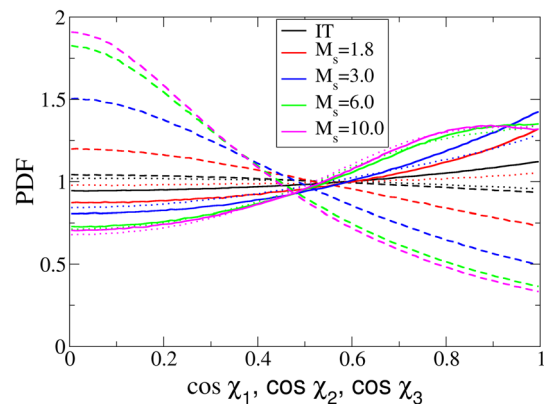

Fig. 11 PDF of cosines of the angles between $\nabla \rho$ and the eigenvectors of **S**: $\cos \chi_1$, *dotted lines*, $\cos \chi_2$, *dashed lines*, $\cos \chi_3$, *solid lines*

in the upstream turbulence, all modes are generated by the interaction. The upstream turbulence data used here are quasi-vortical, with a small dilatational component of less than 1 % kinetic energy. In this case, the density and pressure fluctuations in the upstream fields are correlated, while the temperature fluctuations are smaller. Thus, the pressure and density gradients are mostly aligned (Fig. 10). However, as entropic fluctuations are generated through the shock, this alignment weakens in post-shock turbulence. As a result, the baroclinic contribution to the enstrophy equation increases, while the contribution to the square dilatation equation decreases.

In addition, the shock interaction also changes the alignment between the density gradient and the eigenvectors of the strain rate tensor (Fig. 11). In IT, the density gradient points mostly in the direction of the most compressive (γ-) eigenvector, with no correlation with the other two eigenvectors. This is similar to passive scalar alignment in compressive and incompressible turbulent flows [21,22]. After the interaction with the shock, the density gradient tends to align at a 90° angle with the direction of the α-eigenvector and the align-

ment with the γ-eigenvector weakens. Interestingly, at higher M_s values, as the acoustic field becomes stronger, $\nabla\rho$ starts to have an angle different than zero with the γ-eigenvector.

4 Conclusions

Direct Numerical Simulations (DNS) of shock waves interacting with turbulence are restricted to low Reynolds numbers due to the extremely large meshes required to resolve both the turbulence and the shock. Experimental realizations of this problem are also very challenging, due to problems with controlling the shock wave and the small time and length scales involved in the measurements especially close to the shock front. However, recent high resolution DNS extensively covering the parameter space show that, when there is a large scale separation between the turbulence and the shock width and the turbulence intensity is small, the interaction between a shock wave and isotropic turbulence (IT) can be described by the Linear Interaction Approximation (LIA). Such interaction conditions occur in many practical applications.

In order to study the properties of high Reynolds number post-shock turbulence, LIA was used to generate post-shock fields starting from a forced compressible IT database. This procedure was named Shock-LIA. The database was generated using a 512^3 mesh and a Taylor Reynolds number, $Re_\lambda = 180$, which is much larger than those attained in previous shock–turbulence interaction studies. Here, the case of quasi-vortical turbulence was considered. Since traditional LIA addresses second order moments only, in order to calculate full flow fields, necessary for the higher order moments, the detailed procedure to calculate these fields was given. The main theme of the paper is related to properties of the vorticity field, as a central feature of turbulent flows, and various related quantities. Most of the results presented are in terms of probability density functions (PDFs) of various quantities, which cannot be inferred from the traditional LIA formulas since they require the knowledge of all higher order moments, beyond the variance. The properties of these higher order moments are one of the central open questions in turbulence research.

First, using the DNS database from Ref. [11], it was shown that the vorticity variance from DNS converges to the LIA results as the scale separation increases. The convergence can be obtained even at low upstream Reynolds numbers; however, the properties of the post-shock turbulence change with the Reynolds number. Indeed, the PDF of the strain-enstrophy angle, which changes significantly compared to IT, shows a good match between the DNS and LIA results using the corresponding IT database at $Re_\lambda = 30$, but differences compared to LIA results using the $Re_\lambda = 180$ IT database.

In general, the shock interaction significantly changes the properties of upstream turbulence. Thus, the orientations of vorticity and eigenvectors of the strain rate tensor point to a local axisymmetric state, with a reduced vortex-stretching mechanism on the time scale of the turbulence. In addition, the flexion product becomes inversely correlated to the dilatation in the regions of positive Lamb vector divergence. These changes point to a shock Mach number (M_s) dependent slowing of the return to a fully developed state and increased small scale activity as the turbulence evolves away from the shock. On the other hand, the thermodynamic quantities are also strongly affected by the interaction with the shock. Both acoustic and entropic components are generated even for upstream vortical turbulence and these components propagate with different velocities. The specific correlations between the thermodynamic quantities and the orientations of their gradients depend on the relative strength of these components. Thus, at high M_s values, the orientation between the density gradient and the eigenvectors of the strain rate tensor is very different from that in IT. Again, these are structural changes in post-shock turbulence expected to have a significant effect on the evolution away from the shock.

Finally, we would like to mention that, while shock-resolved DNS remains the gold standard, the results from Ref. [11] highlight the applicability of shock-captured turbulence-resolved simulations and their importance as an accurate tool for shock–turbulence interaction problems, when the scale separation is large enough. However, due to computational limitations, Shock-LIA still can access a region of the parameter space not available to either tools and provide an understanding of the properties of post-shock turbulence in those regimes.

References

1. Ribner, H.S.: Convection of a pattern of vorticity through a shock wave. NACA TR-1164 (1954)
2. Moore, F.K.: Unsteady oblique interaction of a shock wave with a plane disturbance. NACA TR-1165 (1954)
3. Mahesh, K., Lele, S.K., Moin, P.: The influence of entropy fluctuations on the interaction of turbulence with a shock wave. J. Fluid Mech. **334**, 353–379 (1997)
4. Lee, S., Lele, S.K., Moin, P.: Direct numerical simulation of isotropic turbulence interacting with a weak shock wave. J. Fluid Mech. **251**, 533–562 (1993)
5. Jamme, S., Cazalbou, J.B., Torres, F., Chassaing, P.: Direct numerical simulation of the interaction between a shock wave and various types of isotropic turbulence. Flow Turb. Comb. **68**(3), 277–268 (2002)

6. Barre, S., Alem, D., Bonnet, J.P.: Experimental study of a normal shock/homogeneous turbulence interaction. AIAA J. **34**, 968–974 (1996)

7. Lee, S., Lele, S.K., Moin, P.: Interaction of isotropic turbulence with shock waves: Effect of shock strength. J. Fluid Mech. **340**, 225–247 (1997)

8. Agui, J.H., Briassulis, G., Andreopoulos, Y.: Studies of interactions of a propagating shock wave with decaying grid turbulence: velocity and vorticity fields. J. Fluid Mech. **524**, 143–195 (2005)

9. Larsson, J., Lele, S.K.: Direct numerical simulation of canonical shock/turbulence interaction. Phys. Fluids **21**, 126101 (2009)

10. Larsson, J., Bermejo-Moreno, I., Lele, S.K.: Reynolds- and Mach-number effects in canonical shock-turbulence interaction. J. Fluid Mech. **717**, 293–321 (2013)

11. Ryu, J., Livescu, D.: Turbulence structure behind the shock in canonical shock-vortical turbulence interaction. J. Fluid Mech. **756**, R1 (2014)

12. Petersen, M.R., Livescu, D.: Forcing for statistically stationary compressible isotropic turbulence. Phys. Fluids **22**, 116101 (2010)

13. Kovasznay, L.S.G.: Turbulence in supersonic flows. J. Aero. Sci. **20**, 657–674 (1953)

14. Blaisdell, G.A., Mansour, N.N., Reynolds, W.C.: Compressibility effects on the growth and structure of homogeneous turbulent shear flows. J. Fluid Mech. **256**, 443–485 (1993)

15. Livescu, D., Jaberi, F.A., Madnia, C.K.: The effects of heat release on the energy exchange in reacting turbulent shear flow. J. Fluid Mech. **450**, 35–66 (2002)

16. Dimotakis, P.E.: The mixing transition in turbulent flows. J. Fluid Mech. **409**, 69–98 (2000)

17. Johnsen, E., Larsson, J., Bhagatwala, A.V., Cabot, W.H., Moin, P., Olson, B.J., Rawat, P.S., Shankar, S.K., Sjögreen, B., Yee, H.C., Zhong, X., Lele, S.K.: Assessment of high-resolution methods for numerical simulations of compressible turbulence with shock waves. J. Comp. Phys. **229**, 1213–1237 (2010)

18. Livescu, D., Mohd-Yusof, J., Petersen, M.R., Grove, J.W.: CFDNS: a computer code for direct numerical simulation of turbulent flows. Technical report, Los Alamos National Laboratory, LA-CC-09-100 (2009)

19. Kevlahan, N.K., Mahesh, K., Lee, S.: Evolution of the shock front and turbulence structures in the shock/turbulence interaction. Proceedings of Summer Program, CTR, pp. 277–292 (1992)

20. Boratav, O.N., Elghobashi, S.E., Zhong, R.: On the alignment of strain, vorticity and scalar gradient in turbulent, buoyant, non-premixed flames. Phys. Fluids **10**, 2260–2267 (1998)

21. Jaberi, F.A., Livescu, D., Madnia, C.K.: Characteristics of chemically reacting compressible homogeneous turbulence. Phys. Fluids **12**, 1189–1209 (2000)

22. Ashurst, W.T., Kerstein, A.R., Kerr, R.M., Gibson, C.H.: Alignment of vorticity and scalar gradient with strain rate in simulated Navier-Stokes turbulence. Phys. Fluids **30**, 2343–2353 (1987)

23. Vincent, A., Meneguzzi, M.: The spatial structure and statistical properties of homogeneous turbulence. J. Fluid Mech. **225**, 1–20 (1991)

24. Kerr, R.M.: High-order derivative correlations and the alignment of small-scale structures in isotropic numerical turbulence. J. Fluid Mech. **153**, 31–58 (1985)

25. Nomura, K.K., Post, G.K.: The structure and dynamics of vorticity and rate of strain in incompressible homogeneous turbulence. J. Fluid Mech. **377**, 65–97 (1998)

26. Nomura, K.K., Elgobashi, S.E.: The structure of inhomogeneous turbulence in variable density nonpremixed flames. Theor. Comput. Fluid Dyn. **5**, 153–176 (1993)

27. Sinha, K.: Evolution of enstrophy in shock/homogeneous turbulence interaction. J. Fluid Mech. **707**, 74–110 (2012)

28. Hamman, C.W., Klewicki, J.C., Kirby, R.M.: On the Lamb vector divergence in Navier-Stokes flows. J. Fluid Mech. **610**, 261–284 (2008)

29. Robinson, J.C., Rodrigo, J.L., Sadowski, W.: Mathematical Aspects of Fluid Mechanics. Cambridge University Press, Cambridge (2012)

30. Liu, L.Q., Wu, J.Z., Shi, Y.P., Zhu, J.Y.: A dynamic counterpart of Lamb vector in viscous compressible aerodynamics. Fluid Dyn. Res. **46**, 061417 (2014)